WARSAW UNIVERSITY OF TECHNOLOGY Index 351733
FACULTY OF CIVIL ENGINEERING
COMMITTEE FOR CIVIL AND WATER ENGINEERING
POLISH ACADEMY OF SCIENCES ISSN 1230-2945

DOI: 10.24425/ace.2023.144181

ARCHIVES OF CIVIL ENGINEERING

Vol. LXIX ISSUE 1 2023

pp. 421 –436

Research paper

Reinforcement layout design of three-dimensional members under a state of complex stress

Hao Cui[1], Junjie Xia[2], Lang Wu[3], Min Xiao[4]

Abstract: This paper proposes a method to optimize reinforcement layout of three-dimensional members under a state of complex stress and multiple load cases (MLCs). To simulate three-dimensional members, the spatial truss-like material model is adopted. Three families of truss-like members along orthotropic directions are embedded continuously in concrete. The optimal reinforcement layout design is obtained by optimizing the member densities and orientations. The optimal design of three-dimensional member is carried out by solving the problem of minimum volume of reinforcing bars with stress constraints. Firstly, the optimized reinforcement layout under each single load case (SLC) is obtained as per the fully stressed criterion. Second, on the basis of the previous results, an equivalent multi-case optimization is proposed by introducing the idea of stiffness envelope. Finally, according to the characteristics of the truss-like material, a closed and symmetrical surface is adopted to fit the maximum directional stiffness under all SLCs. It can be proved that the densities and orientations of truss-like members are the eigenvalues and eigenvectors of the surface coefficient matrix, respectively. Several three-dimensional members are used as examples to demonstrate the capability of the proposed method in finding the best reinforcement layout design of each reinforced concrete (RC) member and to verify its efficiency in application to real design problems.

Keywords: topology optimization, truss-like material, reinforcement layout, multiple load cases, complex stress

[1]PhD., College of Civil Engineering and Architecture, Jiangxi Science and Technology Normal University, No.605 Fenglin Avenue, 330013, Nanchang, China, e-mail: cuihaoch@qq.com, ORCID: 0000-0002-8292-9555

[2]B. Eng., College of Civil Engineering and Architecture, Jiangxi Science and Technology Normal University, No.605 Fenglin Avenue, 330013, Nanchang, China, e-mail: 2897152269@qq.com, ORCID: 0000-0002-5993-6474

[3]PhD., College of Civil Engineering and Architecture, Jiangxi Science and Technology Normal University, No.605 Fenglin Avenue, 330013, Nanchang, China, e-mail: wulang19812005@126.com, ORCID: 0000-0001-9985-6578

[4]PhD., College of Civil Engineering and Architecture, Jiangxi Science and Technology Normal University, No.605 Fenglin Avenue, 330013, Nanchang, China, e-mail: xmhdts@qq.com, ORCID: 0000-0001-8078-6119

1. Introduction

It is well known that the cross-sectional strain of a rod can be approximated as a linear distribution along the height of the cross-section when the cross-sectional dimension of the rod is much smaller than its length. By introducing the plane-section assumption, the design of the cross-section can be perfectly solved, and the member or part that does not conform to the assumption becomes a difficult problem. According to it, an rc structure can be categorized into b-regions (Bernoulli regions) and d-regions (discontinuity regions) in practical design processes. The approach for b-region design is maturely established and can be easily achieved by the traditional bending theory and a general shear design method. While in the structural design for d-regions, traditional approaches for slender beams are inappropriate. The failure mode in d-regions is normally presented as shear failure rather than flexural failure. Therefore, how to achieve a proper analysis and design for complex stress components such as corbels, walls or deep beams with openings, pile caps, and beam-column joints has been an enormous challenge for decades.

Although relevant design codes of practice provide general design methods for complex stress components, these methods are usually semi-experiential and semi-theoretical ones based on the plane-section assumption. A reinforcement layout design is even based entirely on empirical formulas. This may lead to a conservative or unsafe design. At present, it is widely recognized that the strut-and-tie method is a basic tool for the analysis and design of RC structures, which has been incorporated in different codes of practice. However, models created by the method are not unique and tend to depend on experience and intuition of the designers. It is particularly true for d-regions of the structure, where the load path distribution is non-linear. Sometimes, it is almost impossible to determine correct strut-and-tie models (STMS) in RC structures with complicated geometry and loading conditions. Consequently, we must consider other methods and tools.

Topology optimization technique as an efficient tool has attracted much attention from both academic and industrial engineering community. Several approaches have been put forward to solve topology optimization problems so far [1]. They can be used to optimize the design of plane structures, space structures and prager structures [2]. In recent years, some new methods have emerged in the field of structural topology optimization. Guo et al. [3] proposed the moving morphable components (MMC) method. Its basic idea is to realize structural topology optimization through a series of actions such as rotation, movement and merging of deformable components. Similar to this method, there is moving morphable bars method [4].

With the development of topology optimization techniques, topology optimization was introduced to generate STMS. Some scholars adopted the eso method to generate STMS [5–9]. Shobeiri et al. [10, 11] used the beso algorithm to generate STMS. In the preceding research, the reinforced concrete is regarded as a single material, and the unnecessary materials are removed using the eso or beso algorithm to obtain the optimal truss layout. The compression members in the truss represent concrete and the tension members represent reinforcing bars. Bruggi [12] established STMS by solving the problem of minimum flexibility with volume constraints based on the simp method. Xia et al. [13]

proposed a program to evaluate the topology optimization results of generating STMS. Giao et al. [14] established STMS by solving the problem of minimizing the flexibility with volume constraints using the mmc method. However, the preceding methods did not take into account the differences between the characteristics of two materials, which is different from the actual stress state of RC members. Victoria et al. [15] presented a method for generating more efficient STMS considering the different mechanical properties for the tensile (steel) and compressive (concrete) regions. Du et al. [16] developed structural topology optimization involving different material properties in tension and compression, which can be used for generating STMS. Amir and Sigmund [17] proposed an optimization method combining a continuum and the ground structure approach to generate the optimal reinforcement distribution. Based on the idea of the ground structure, the method uses the truss topology optimization method to find the best truss (reinforcement) layout. however, the drawback of this method is that the final layout for reinforcing bars is dominantly influenced by the predefined truss layout. Luo and Kang [18] developed a topology optimization method using bi-material model. The optimal reinforcement design of RC structures is carried out by solving the problem of minimum structural flexibility with concrete drucker prager stress constraints and reinforcement volume constraints. Yang et al. [19] used truss-like topology optimization to optimize the reinforcement design of RC structures under an SLC. This paper proposes a method to optimize the reinforcement layout of three-dimensional members under a state of complex stress and an MLC. The idea here is a further extension of the previous work [20].

The sequel of this paper is organized as follows. Section 2 introduces the elastic matrix of the spatial truss-like material and the directional stiffness. Section 3 introduces finite element analysis. The principal stress and principal stress direction of composite materials are obtained in Section 4. To optimize reinforcement layout under an MLC is presented in Section 5. Section 6 introduces the procedure for the reinforcement layout design of three-dimensional members. Two numerical examples are illustrated in Section 7. Conclusions and future perspectives are outlined in Section 8.

2. Directional stiffness of truss-like material

The spatial truss-like material model with three families of orthotropic members is adopted to simulate reinforcing bars embedded in concrete. It is assumed that the densities and orientations of the three families of reinforcing bars are ρ_1,ρ_2 and ρ_3, and the orientation vectors of reinforcing bars in the structural coordinate system are $\boldsymbol{l}_1, \boldsymbol{l}_2$ and $\boldsymbol{l}_3$.The orientation vectors can be written as

$$\boldsymbol{l}_b = \sum_{i=1}^{3} l_{bi}\boldsymbol{e}_i, \quad (b = 1, 2, 3) \tag{2.1}$$

where the direction cosines l_{b1}, l_{b2} and l_{b3} are given by $l_{bi} = \cos(\boldsymbol{e}_i, \boldsymbol{l}_b)$.

The elastic matrix of the spatial truss-like material can be written as follows [21]

$$\boldsymbol{D}_s(\rho_1,\rho_2,\rho_3,\boldsymbol{l}1,\boldsymbol{l}2,\boldsymbol{l}3) = E_s\sum_{b=1}^{3}\rho_b\sum_{r=1}^{6}g_r(\boldsymbol{l}_b)\mathbf{A}_r \tag{2.2}$$

where: g_r – the component of the functional vector $\boldsymbol{g}$, $\boldsymbol{A}_r$ – being the constant matrix, E_s – Young's modulus of reinforcing bars.

The elastic matrix at any point within an element e is calculated as follows

$$\boldsymbol{D}_e(\xi,\eta,\zeta) = \sum_{j\in S_e}N_j(\xi,\eta,\zeta)\boldsymbol{D}_s(\rho_{1j},\rho_{2j},\rho_{3j},\boldsymbol{l}_{1j},\boldsymbol{l}_{2j},\boldsymbol{l}_{3j}) \tag{2.3}$$

where: $N_j(\xi,\eta,\zeta)$ – the shape function, S_e – the set of nodes belonging to element e.

According to Eq. (2.3), the directional stiffness along $\boldsymbol{e}_1$ is denoted as

$$S(\boldsymbol{e}_1) = D_{11} = E_s\sum_{b=1}^{3}l_{b1}^2\rho_b = E_s\sum_{b=1}^{3}(\boldsymbol{e}_1\cdot\boldsymbol{l}_b)^2\rho_b \tag{2.4}$$

Based on Eq. (2.4), we can obtain the directional stiffness along any unit vector $\boldsymbol{x}$

$$S(\boldsymbol{x}) = E_s\sum_{b=1}^{3}(\boldsymbol{x}\cdot\boldsymbol{l}_b)^2\rho_b = E_s\sum_{i=1}^{3}\sum_{j=1}^{3}\left(\sum_{b=1}^{3}l_{bi}l_{bj}\rho_b\right)x_ix_j = E_s\boldsymbol{x}^{\mathrm{T}}\boldsymbol{C}\boldsymbol{x} \tag{2.5}$$

where

$$[\boldsymbol{C}]_{ij} = \sum_{b=1}^{3}l_{bi}l_{bj}\rho_b \tag{2.6}$$

It is easily verified that $[\boldsymbol{C}]_{ij} = [\boldsymbol{C}]_{ji}$ and $\boldsymbol{C}$ is a real symmetric matrix. Therefore, there exists an orthogonal matrix $\boldsymbol{Q}$ such that $\boldsymbol{Q}^T\boldsymbol{C}\boldsymbol{Q}$ is diagonal.

$$\boldsymbol{Q}^T\boldsymbol{C}\boldsymbol{Q} = \mathrm{diag}[\lambda_1,\lambda_2,\lambda_3] \tag{2.7}$$

where λ_1, λ_2 and λ_3 are the eigenvalues of $\boldsymbol{C}$. From Eq. (2.7), we have

$$\boldsymbol{C} = \boldsymbol{Q}\mathrm{diag}[\lambda_1,\lambda_2,\lambda_3]\boldsymbol{Q}^T \tag{2.8}$$

Then we can get

$$S(\boldsymbol{x}) = E_S\boldsymbol{x}^T\boldsymbol{Q}\mathrm{diag}[\lambda_1,\lambda_2,\lambda_3]\boldsymbol{Q}^T\mathbf{x} = E_S(\boldsymbol{Q}^T\boldsymbol{x})^T\,\mathrm{diag}[\lambda_1,\lambda_2,\lambda_3]\boldsymbol{Q}^T\boldsymbol{x} \tag{2.9}$$

Assume that $\lambda_1\geq\lambda_2\geq\lambda_3$, and suppose that

$$(\boldsymbol{Q}^T\boldsymbol{x})^T = [a_1,a_2,a_3] \tag{2.10}$$

Substituting Eq. (2.10) into Eq. (2.9), it can be concluded that

$$S(\boldsymbol{x}) = E_S\sum_{i=1}^{3}\lambda_ia_i^2 \leq E_S\lambda_1\sum_{i=1}^{3}a_i^2 = E_S\lambda_1(\boldsymbol{Q}^{\mathrm{T}}\boldsymbol{x})^{\mathrm{T}}(\boldsymbol{Q}^{\mathrm{T}}\boldsymbol{x}) = E_S\lambda_1\boldsymbol{x}^{\mathrm{T}}\boldsymbol{x} = E_S\lambda_1 \tag{2.11}$$

Similarly, we have $S(\boldsymbol{x}) \geq E_S \lambda_3$. Hence, it can be obtained that

$$E_s \lambda_3 \leq S(x) \leq E_s \lambda_1 \tag{2.12}$$

According to the characteristics of the spatial truss-like material model, the directional stiffness $S(\boldsymbol{x})$ along unit vector $\boldsymbol{l}_b$ $(b = 1, 2, 3)$ has three local maxima $E_s t_b$ $(b = 1, 2, 3)$. It is assumed that

$$\rho_1 \geq \rho_2 \geq \rho_3 \tag{2.13}$$

Then, we get

$$E_s \rho_3 \leq S(x) \leq E_s \rho_1 \tag{2.14}$$

From Eq. (2.12) and (2.14), we have $\lambda_1 = \rho_1, \lambda_3 = \rho_3$. Moreover, it is easily verified that

$$\mathrm{Tr}(\boldsymbol{C}) = \sum_{b=1}^{3} \rho_b = \sum_{b=1}^{3} \lambda_b \tag{2.15}$$

Then, we get $\lambda_2 = \rho_2$. Therefore, it is concluded that the eigenvalues of $\boldsymbol{C}$ are just identical to densities of reinforcing bars at nodes and three families of orthotropic reinforcing bars are aligned with the eigenvectors.

3. Finite element analysis and steel bars volume

To simulate RC members, the spatial truss-like material model with three families of orthotropic members is adopted, in which three families of members along three orthotropic directions are embedded continuously in concrete. The finite element analysis used in the algorithm regards all materials as linear elastic. A RC member under unidirectional stress is shown in Fig. 1.

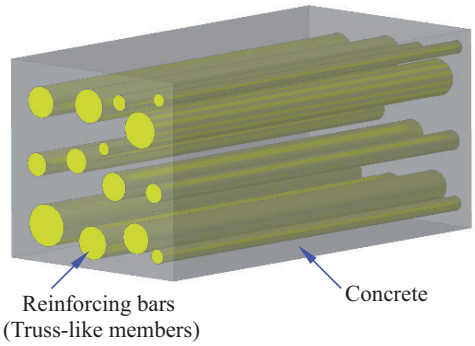

Fig. 1. Member under unidirectional stress

The element stiffness matrix of the RC member can be written as

$$\boldsymbol{k}_e = \int_{V_e} \boldsymbol{B}^T (\boldsymbol{D}_s + \boldsymbol{D}_c)\boldsymbol{B}\,\mathrm{d}V = \boldsymbol{k}_e^s + \boldsymbol{k}_e^c \tag{3.1}$$

where: $\boldsymbol{D}_c$ – the elastic matrix of concrete, $\boldsymbol{D}_s$ – the elastic matrix of continua of reinforcing bars, $\boldsymbol{B}$ – the geometry matrix, $\boldsymbol{k}_e^s$ – the element stiffness matrix of continua of reinforcing bars, $\boldsymbol{k}_e^c$ – the element stiffness matrix of concrete.

$$\boldsymbol{k}_e^s = \sum_{j\in S_e}\sum_{b=1}^{3}\rho_{bj}\sum_{r=1}^{6} g_r(\boldsymbol{l}_{bj})\boldsymbol{H}_{ejr} \tag{3.2}$$

where $\boldsymbol{H}_{ejr}$ is a constant matrix (see [21] for details).

The structural stiffness matrix $\boldsymbol{K}$ of the RC member can be obtained

$$\boldsymbol{K} = \sum_e (\boldsymbol{k}_e^s + \boldsymbol{k}_e^c) \tag{3.3}$$

It is reasonable to assume that no slip occurs at the interface between reinforcing bars and concrete by the aid of the bond stress along the concrete-steel interface. Namely, the strain at node j is determined from the following equation

$$\varepsilon_j = \frac{1}{n_j}\sum_{e\in S_j}\boldsymbol{B}_j\boldsymbol{U}_e \tag{3.4}$$

where S_j and n_j are the set of elements and the number of elements around node j, respectively.

The stress vector of reinforcing bars and concrete is obtained as follows, respectively.

$$\boldsymbol{\sigma}^s = \boldsymbol{D}_s\boldsymbol{\varepsilon}, \quad \boldsymbol{\sigma}^c = \boldsymbol{D}_c\boldsymbol{\varepsilon} \tag{3.5}$$

The volume of reinforcing bars is calculated by the following equation

$$V = \sum_e\sum_{b=1}^{3}\int_{V_e}\sum_{j\in S_e} N_j\rho_{bj}\,\mathrm{d}V \tag{3.6}$$

4. Principal stress and principal stress direction of composite materials

The global coordinate system Oxy and the local one $O\overline{xy}$ are presented in Fig. 2. Reinforcing bars are arranged along the coordinate axes of $O\overline{xy}$. The stress components are defined on the three-dimensional differential element which is taken from the composite material, and thus the stress vectors in the local one are given by

$$\overline{\boldsymbol{\sigma}}^s = [\sigma_{\overline{x}}^s \quad \sigma_{\overline{y}}^s \quad \sigma_{\overline{z}}^s \quad \tau_{\overline{yz}}^s \quad \tau_{\overline{zx}}^s \quad \tau_{\overline{xy}}^s]^T \tag{4.1}$$

Then the stress transformation can be expressed as follow

$$\overline{\boldsymbol{\sigma}}^s = \boldsymbol{T}_\sigma \boldsymbol{\sigma}^s \tag{4.2}$$

where $\boldsymbol{T}_\sigma$ is the transformation matrix for stress.

The stress components in the global coordinate system can be written as

$$\boldsymbol{\sigma}^s = [\sigma_x^s \quad \sigma_y^s \quad \sigma_z^s \quad \tau_{yz}^s \quad \tau_{zx}^s \quad \tau_{xy}^s]^T = \boldsymbol{T}_\sigma^{-1}\overline{\boldsymbol{\sigma}}^s = \boldsymbol{T}_\varepsilon^T \overline{\boldsymbol{\sigma}}^s \tag{4.3}$$

where $\boldsymbol{T}_\varepsilon$ is the transformation matrix for strain.

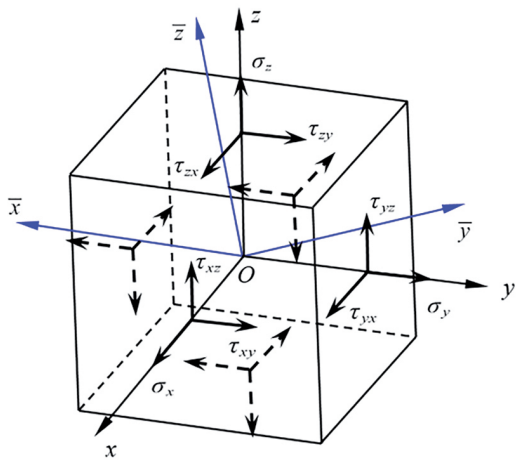

Fig. 2. Three-dimensional differential element

As is known, the members in the truss-like continuum are arranged along the direction of principal stress under an SLC. Namely, $\tau_{\overline{yz}} = \tau_{\overline{zx}} = \tau_{\overline{xy}} = 0$. Substituting it into Eq. (4.3), we get

$$\begin{bmatrix} \sigma_x^s \\ \sigma_y^s \\ \tau_{xy}^s \end{bmatrix} = \begin{bmatrix} l_{11}^2 & l_{21}^2 & l_{31}^2 \\ l_{12}^2 & l_{22}^2 & l_{32}^2 \\ l_{13}^2 & l_{23}^2 & l_{33}^2 \end{bmatrix} \begin{bmatrix} \sigma_{\overline{x}}^s \\ \sigma_{\overline{y}}^s \\ \tau_{\overline{xy}}^s \end{bmatrix} \tag{4.4}$$

The strain along reinforcing bars reaches the allowable strain as per the fully stressed criterion during each iteration. According to the stress-strain relationship of truss like members, the normal stress components in the local coordinate system can be denoted as

$$\sigma_{\overline{x}}^s = E_s \rho_{\overline{x}}^s \varepsilon_p^s, \quad \sigma_{\overline{y}}^s = E_s \rho_{\overline{y}}^s \varepsilon_p^s, \quad \sigma_{\overline{z}}^s = E_s \rho_{\overline{z}}^s \varepsilon_p^s \tag{4.5}$$

where $\rho_{\overline{x}}^s$, $\rho_{\overline{y}}^s$ and $\rho_{\overline{z}}^s$ is density components of reinforcing bars in the local coordinate system. Similarly, the normal stress components in the global one can be written as

$$\sigma_x^s = E_s \rho_x^s \varepsilon_p^s, \quad \sigma_y^s = E_s \rho_y^s \varepsilon_p^s, \quad \sigma_z^s = E_s \rho_z^s \varepsilon_p^s \tag{4.6}$$

where ρ_x^s, ρ_y^s and ρ_z^s denote density components of reinforcing bars in the global coordinate system. Substituting Eq. (4.5) and (4.6)into Eq. (4.4), we get

$$\begin{bmatrix} \rho_x^s \\ \rho_y^s \\ \rho_z^s \end{bmatrix} = \begin{bmatrix} l_{11}^2 & l_{21}^2 & l_{31}^2 \\ l_{12}^2 & l_{22}^2 & l_{32}^2 \\ l_{13}^2 & l_{23}^2 & l_{33}^2 \end{bmatrix} \begin{bmatrix} \rho_{\overline{x}}^s \\ \rho_{\overline{y}}^s \\ \rho_{\overline{z}}^s \end{bmatrix} \tag{4.7}$$

It is assumed that the areas of the x-face, y-face and z-face of the differential element are $\mathrm{d}A_x$, $\mathrm{d}A_y$ and $\mathrm{d}A_z$, respectively. Consider x-direction equilibrium

$$\mathrm{d}F_x = \sigma_x^s \rho_x^s \mathrm{d}A_x + \sigma_x^c (1 - \rho_x^s) \mathrm{d}A_x \tag{4.8}$$

This leads to

$$\sigma_x = \sigma_x^s \rho_x^s + \sigma_x^c (1 - \rho_x^s) \tag{4.9}$$

Similarly, we have

$$\sigma_y = \sigma_y^s \rho_y^s + \sigma_y^c (1 - \rho_y^s), \quad \sigma_z = \sigma_z^s \rho_z^s + \sigma_z^c (1 - \rho_z^s) \tag{4.10}$$

The average shear stress is as follows

$$\tau_{yz} = \tau_{yz}^s \rho_y^s + \tau_{yz}^c (1 - \rho_y^s), \quad \tau_{zx} = \tau_{zx}^s \rho_z^s + \tau_{zx}^c (1 - \rho_z^s), \quad \tau_{xy} = \tau_{xy}^s \rho_x^s + \tau_{xy}^c (1 - \rho_x^s) \tag{4.11}$$

Then we can establish the principal value problem and solve the characteristic equation to explicitly determine the principal values and directions. The general characteristic equation for the stress tensor is as follow

$$\sigma^3 - J_1 \sigma^2 + J_2 \sigma - J_3 = 0 \tag{4.12}$$

where J_1, J_2 and J_3 are the fundamental invariants of the stress tensor.

5. Envelope of directional stiffness and optimizing reinforcement layout

The optimal reinforcement layout under an MLC are obtained on the basis of the optimization results under each SLC. Therefore, it is necessary to optimize reinforcement layout under each SLC first. The optimization problem under each SLC can be described as

$$\begin{cases} \text{find} & \overline{\rho}_{bj}, \overline{\boldsymbol{l}}_{bj} & \\ \min & \overline{V} & \\ \text{s.t.} & \left|\sigma_b^s\right| \le \sigma_{\mathrm{p}}^s & b = 1, 2, 3 \\ & \left|\sigma_c^c\right| \le \sigma_{\mathrm{pc}}^c & j = 1, 2, \cdots, J \\ & \sigma_t^c \le \sigma_{\mathrm{pt}}^c & \end{cases} \tag{5.1}$$

where: $\overline{\rho}_{bj}$ – the densities of reinforcing bars at node j under each SLC, $\bar{\boldsymbol{l}}_{bj}$ – the orientations of reinforcing bars at node j under each SLC, $\sigma_{\mathrm{p}}^{\mathrm{s}}$ – allowable stress of reinforcement bars, $\sigma_{\mathrm{pc}}^{\mathrm{c}}$ – allowable compressive stress of concrete, $\sigma_{\mathrm{pt}}^{\mathrm{c}}$ – allowable tensile stress of concrete, $\overline{V}$ – the volume of reinforcement bars under each SLC, σ_b^s – stress along reinforcement bars, σ_c^c and σ_t^c – principal stress in concrete.

The optimal densities of reinforcement bars under each SLC are optimized as per the fully stressed criterion

$$\overline{\rho}_{bj}^{k+1} = \frac{\left|\sigma_{bj}^{k}\right| - \sigma_p^c}{\sigma_{\mathrm{p}}^s - \sigma_p^c}, \quad \begin{array}{l} \sigma_p^c = \sigma_{pt}^c, \text{ if } \varepsilon_b^k \geq 0, \ b = 1,2,3 \\ \sigma_p^c = \sigma_{pc}^c, \text{ if } \varepsilon_b^k < 0, \ j = 1,2,\cdots,J \end{array} \tag{5.2}$$

where: σ_{bj}^k – principal stress of the concrete-steel composite, ε_b^k – principal strain under each SLC, k – the iterative index. The reinforcement bars are aligned with the principal stress directions.

Once the optimal distribution of reinforcing bars in concrete is obtained, the directional stiffness along any direction under SLC L is determined according to Eq. (2.5). The maximum stiffness over all directions under all SLCs is

$$S_m(\boldsymbol{x}) = E_s \max_L \sum_{b=1}^{3} \left(\sum_{i=1}^{3} x_i \bar{l}_{bijL} \right)^2 \overline{\rho}_{bjL}, \quad L = 1,2,\cdots,L_c \tag{5.3}$$

According to Eq. (2.5), the directional stiffness of spatial truss-like structures can be described by a closed surface. Therefore, the directional stiffness of the optimal structure under an MLC is assumed as

$$\begin{aligned} S(\boldsymbol{x}) &= \boldsymbol{P}(\boldsymbol{x})\overline{\boldsymbol{C}} = \boldsymbol{x}^{\mathrm{T}}\boldsymbol{C}\boldsymbol{x}; \ |\boldsymbol{x}| = 1 \\ \overline{\boldsymbol{C}} &= \begin{bmatrix} c_1 & c_2 & c_3 & c_4 & c_5 & c_6 \end{bmatrix}^{\mathrm{T}} \\ \boldsymbol{P}(\boldsymbol{x}) &= \begin{bmatrix} x_1^2 & x_2^2 & x_3^2 & 2x_1x_2 & 2x_2x_3 & 2x_3x_1 \end{bmatrix} \\ \boldsymbol{C} &= \begin{bmatrix} c_1 & c_4 & c_6 \\ c_4 & c_2 & c_5 \\ c_6 & c_5 & c_3 \end{bmatrix} \end{aligned} \tag{5.4}$$

where c_1–c_6 are unsolved real coefficients.

To minimize total volume of reinforcing bars, Eq. (5.4) is adopted to fit the maximum directional stiffness under all SLCs and it is reasonable to ensure that the directional stiffness under MLC is as close as possible to the maximum directional stiffness of the optimal structure under every SLC along all directions. Then the optimal reinforcement layout under an MLC can be equivalent to solving a least squares problem. The coefficient vector $\overline{\boldsymbol{C}}$ in Eq. (5.4) can be determined [22].

$$\overline{\boldsymbol{C}} = \left[\oiint_{S_0} \boldsymbol{P}^{\mathrm{T}}(\boldsymbol{x})\boldsymbol{P}(\boldsymbol{x})\mathrm{dA} \right]^{-1} \oiint_{S_0} \boldsymbol{P}^{\mathrm{T}}(\boldsymbol{x}) S_m(\boldsymbol{x})\mathrm{dA} \tag{5.5}$$

where S_0 is the integral domain, a unit sphere surface that can represent any direction. The second surface integral at the right end of the Eq. (5.5) is calculated by numerical method

$$\begin{aligned}(5.6)\qquad \oiint_{S_0} \boldsymbol{P}^{\mathrm{T}}(\boldsymbol{x})S_m(\boldsymbol{x})\mathrm{dA} &= 2\int_0^{\pi}\int_0^{\pi} \boldsymbol{P}^{\boldsymbol{T}}(\boldsymbol{x})S_m(\boldsymbol{x})\sin\varphi\,\mathrm{d}\theta\,\mathrm{d}\varphi \\ &= 2\sum_{i=1}^{n_\theta}\sum_{j=1}^{n_\varphi}\boldsymbol{P}^{\mathrm{T}}(\boldsymbol{r}_{ij})S_m(\boldsymbol{r}_{ij})\sin\varphi_j\Delta\theta\Delta\varphi \\ &= \frac{2\pi^2}{n_\theta n_\varphi}\sum_{i=1}^{n_\theta}\sum_{j=1}^{n_\varphi}\boldsymbol{P}^{\mathrm{T}}(\boldsymbol{r}_{ij})S_m(\boldsymbol{r}_{ij})\sin\varphi_j\end{aligned}$$

where $\boldsymbol{r}_{ij}$ is the unit vector in the spherical coordinate.

$$(5.7)\qquad \boldsymbol{r}_{ij} = [\sin\varphi_j\cos\theta_i \quad \sin\varphi_j\sin\theta_i \quad \cos\varphi_j]^{\mathrm{T}}$$

And the integral intervals of integral variables θ and φ are equally divided into n_θ and n_φ parts, respectively.

Then the real symmetric matrix $\boldsymbol{C}$ is determined. According to the previous discussion, the optimal reinforcement layout of members under the MLC is obtained by solving the eigenvalues problem of the coefficient matrix $\boldsymbol{C}$ of the surface.

6. Optimization approach and procedure

The procedure for the reinforcement layout design of three-dimensional members under an MLC can be described in following steps.

1. The design domain is divided into finite elements.
2. Set the iteration index $k = 0$; Initial design values is assigned to design variables.
3. Finite element analysis is performed.
4. The stress vectors of reinforcing bars and concrete is calculated according to Eq. (3.5).
5. The density components of reinforcing bars are calculated in the global coordinate system according to Eq. (4.7).
6. The stress tensor of composite material is obtained by Eq. (4.9) and (4.10).
7. Determine the average principal stress and principal stress direction according to Eq. (4.12).
8. The optimal reinforcement layout under each SLC is determined by Eq. (5.2).
9. Eq. (5.4) is used to fit the maximum directional stiffness under all SLCs.
10. Find the eigenvalues and eigenvectors of the coefficient matrix $\boldsymbol{C}$, which are taken as the optimal densities and orientations, respectively, of reinforcing bars under the MLC.
11. Return to step (3) if the relative change in the maximum densities of reinforcing bars in two successive iterations is larger than a given small positive value or the loop iterations are less than 10. Otherwise, the iterations are terminated.

7. Numerical examples

Two examples are presented in this section. The concrete grade is C30. Young's modulus of reinforcement bars and concrete are $E_s = 210$ GPa and $E_c = 7.15$ GPa, respectively. Poisson's ratio of concrete is $\nu = 0.2$; the compressive and tensile strengths of concrete are $\sigma^c_{pc} = 14.3$ MPa and $\sigma^c_{pt} = 1.43$ MPa, respectively. The compressive and tensile strengths of reinforcement bars are $\sigma^s_p = 360$ MPa. Hexahedron elements with 8 nodes are adopted. Crossed lines at nodes are used to denote the optimal layout of reinforcement bars. The orientations and the lengths of the three lines represent the orientations and densities of three families of reinforcement bars at every node. Some lines that are too long are cut short to make the figure distinguishable.

Example 1: In this example, the layout design of reinforcement bars in an L-shape column is considered. The geometry and dimensions of the design domain are shown in Fig. 3a. The bottom surface is fixed and three independent load sets $P_1 = 1000$ kN, $P_2 = 300$ kN and $P_3 = 300$ kN are applied to the middle point of the right surface. Crossed lines are drawn in Fig. 3b, 3c and 3d, Fig. 4a, 4b, 4c and 4d, Fig. 5a, 5b, 5c and 5d, Fig. 6a, 6b, 6c and 6d, to demonstrate the optimal layout of the reinforcement bars under the SLC1 ($P_1 = 1000$ kN), SLC2 ($P_2 = 300$ kN), SLC3 ($P_3 = 300$ kN) and MLC ($P_1 = 1000$ kN, $P_2 = 300$ kN, $P_3 = 300$ kN), respectively.

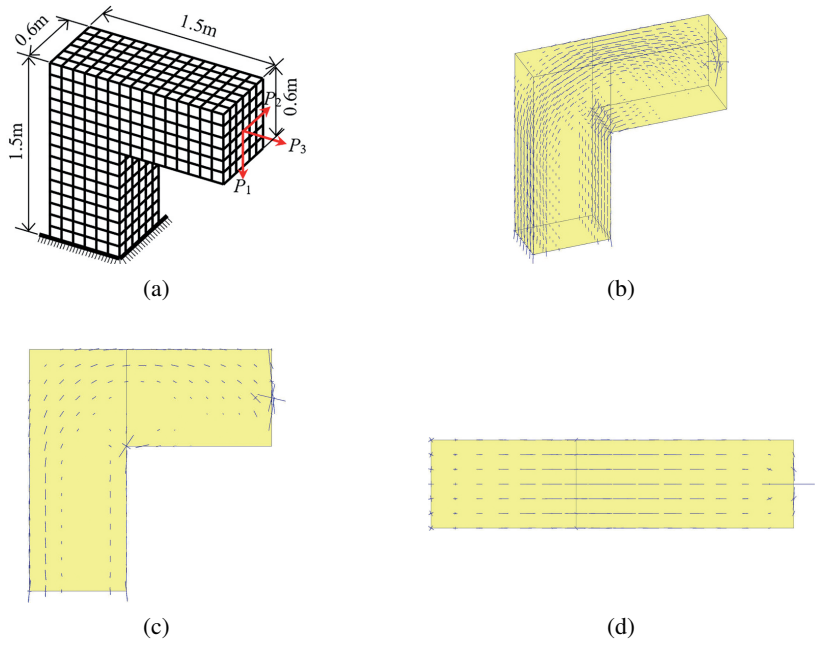

Fig. 3. Optimal layout of reinforcing bars under SLC1 of example 1: (a) mechanics model; (b) analysis results; (c) front view; (d) vertical view

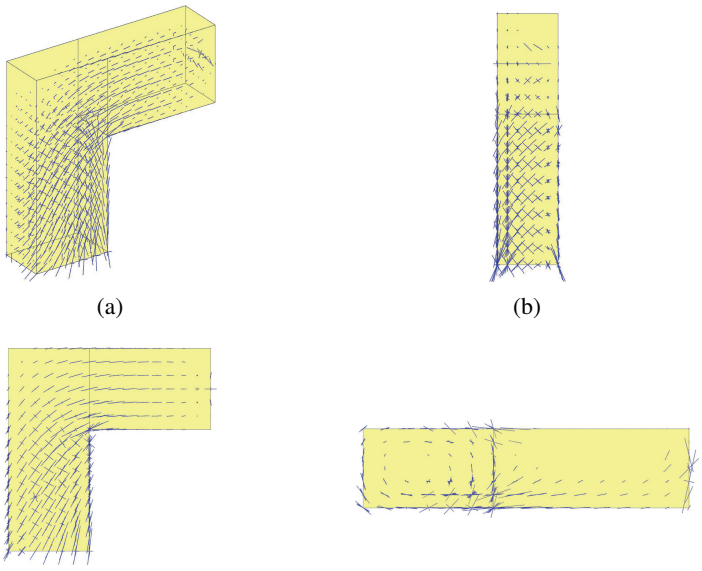

(a) (b)

(c) (d)

Fig. 4. Optimal layout of reinforcing bars under SLC2 of example 1: (a) analysis results; (b) right view; (c) front view; (d) vertical view

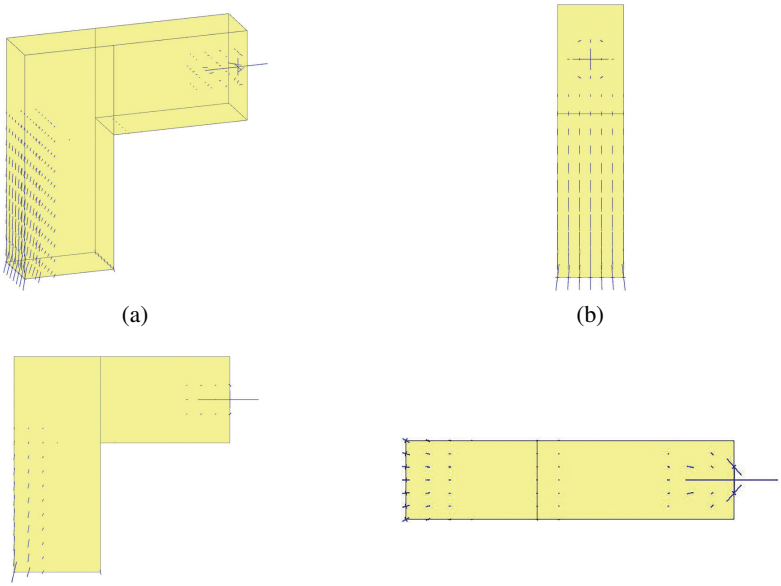

(a) (b)

(c) (d)

Fig. 5. Optimal layout of reinforcing bars under SLC3 of example 1: (a) analysis results; (b) right view; (c) front view; (d) vertical view

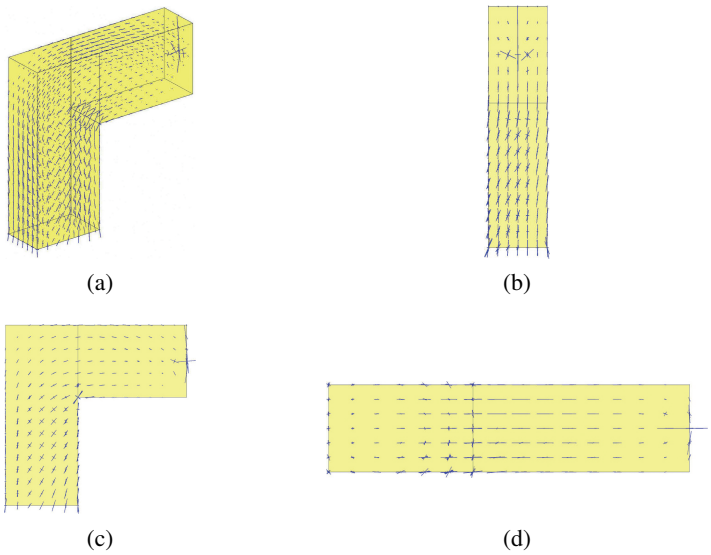

(a) (b) (c) (d)

Fig. 6. Optimal layout of reinforcing bars under MLC of example 1: (a) analysis results; (b) right view; (c) front view; (d) vertical view

Example 2: In this example, the layout design of reinforcing bars in a short cantilever beam with three openings is considered. The geometry and dimensions of the design domain are shown in Fig. 7a. The left surface is fixed and two independent load sets $P_1 = 400$ kN and $P_2 = 100$ kN are applied to the middle point of the right surface. Crossed lines are drawn in Fig. 7a, 7b, 7c and 7d, Fig. 8a, 8b, 8c and 8d, Fig. 9a, 9b, 9c and 9d, to demonstrate the optimal layout of reinforcement bars under the SLC1 ($P_1 = 400$ kN), SLC2 ($P_2 = 100$ kN) and MLC ($P_1 = 400$ kN, $P_2 = 100$ kN), respectively.

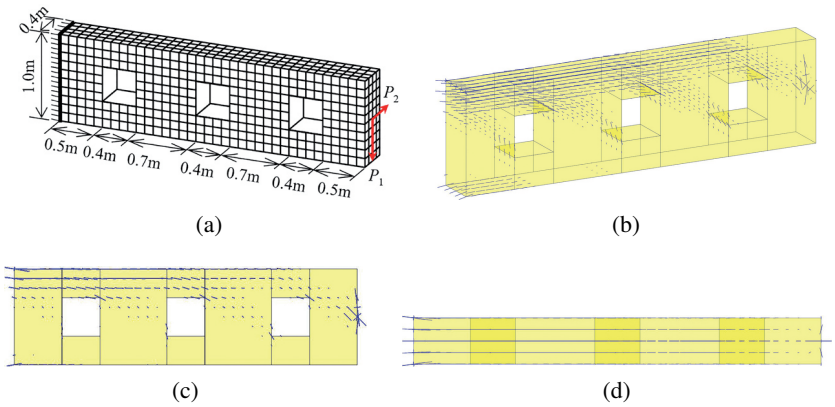

(a) (b) (c) (d)

Fig. 7. Optimal layout of reinforcing bars under SLC1 of example 2: (a) mechanics model; (b) analysis results; (c) front view; (d) vertical view

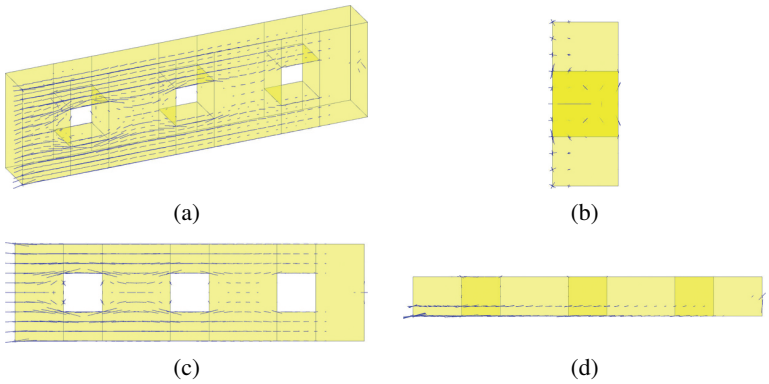

Fig. 8. Optimal layout of reinforcing bars under SLC2 of example 2: (a) analysis results; (b) right view; (c) front view; (d) vertical view

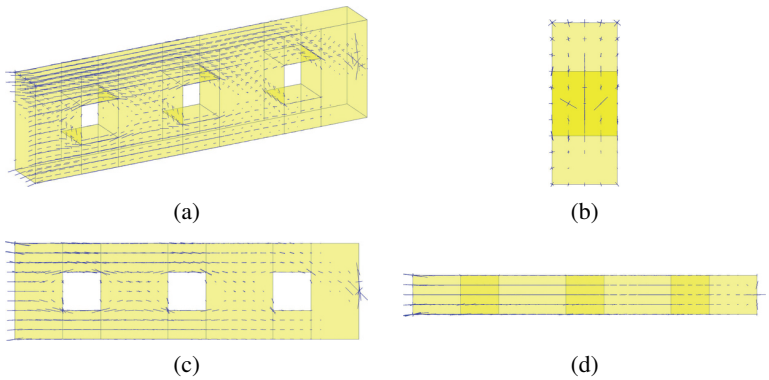

Fig. 9. Optimal layout of reinforcing bars under MLC of example 2: (a) analysis results; (b) right view; (c) front view; (d) vertical view

8. Conclusions

A numerical algorithm is presented in this paper that can generate the optimal reinforcement layout of three-dimensional members under an MLC. To simulate three-dimensional members, the spatial truss-like material model with three families of orthotropic members is adopted, in which three families of members along three orthotropic directions are embedded continuously in concrete. The densities and orientations of the three families of truss-like members at the nodes are optimized. Crossed lines at nodes are used to denote the optimal layout of the reinforcing bars. The orientations and the lengths of the three lines represent the orientations and densities of three families of reinforcement bars at every node. Comparing the STM, the proposed numerical algorithm obtains directly the optimal reinforcement layout of three-dimensional members with fewer elements. It can decrease

the computing cost with fewer iterations. The method proposed in this paper provides a reference for concept design of three-dimensional members under a state of complex stress.

Acknowledgements

The research reported in this paper was financially supported by the Research Project of Science and Technology for Jiangxi Province Department of Education, China (No. GJJ201128), Doctor Start-up Fund of Jiangxi Science & Technology Normal University, China (No. 2020BSQD018) and the Humanities and Social Sciences Research Project (No. GL21118).

References

[1] O. Sigmund and K. Maute, "Topology optimization approaches", *Structural and Multidisciplinary Optimization*, vol. 48, no. 6, pp. 1031–1055, 2013, DOI: 10.1007/s00158-013-0978-6.

[2] G. Dzierżanowski and K. Hetmański, "Optimal design of archgrids: the second-order cone programming perspective", *Archives of Civil Engineering,* vol. 67, no. 4, pp. 469–486, 2021, DOI: 10.24425/ace.2021.138512.

[3] X. Guo, W. Zhang, and W. Zhong, "Doing topology optimization explicitly and geometrically—a new moving morphable components based framework", *Journal of Applied Mechanics*, vol. 81, no. 8, art. no. 081009, 2014, DOI: 10.1115/1.4027609.

[4] V.N. Hoang and G.W. Jang, "Topology optimization using moving morphable bars for versatile thickness control", *Computer Methods in Applied Mechanics and Engineering*, vol. 317, pp. 153–173, 2017, DOI: 10.1016/j.cma.2016.12.004.

[5] Q.Q. Liang, Y.M. Xie, and G.P. Steven, "Topology optimization of strut-and-tie models in reinforced concrete structures using an evolutionary procedure", *ACI Structural Journal*, vol. 97, no. 2, pp. 322–331, 2000.

[6] Q.Q. Liang, Y.M. Xie, and G.P. Steven, "Generating optimal strut-and-tie models in prestressed concrete beams by performance-based optimization", *ACI Structural Journal*, vol. 98, no. 2, pp. 226–232, 2001.

[7] H.G. Kwak and S.H. Noh, "Determination of strut-and-tie models using evolutionary structural optimization", *Engineering Structures*, vol. 28, no. 10, pp. 1440–1449, 2006, DOI: 10.1016/j.engstruct.2006.01.013.

[8] R.M. Lanes, M. Greco, and M.B.B.F. Guerra, "Strut-and-tie models for linear and nonlinear behavior of concrete based on topological evolutionary structure optimization (ESO) ", *Revista IBRACON de Estruturas e Materiais*, vol. 12, no. 1, pp. 87–100, 2019, DOI: 10.1590/S1983-41952019000100008.

[9] L.J. Leu, C.W. Huang, C.S. Chen, et al., "Strut-and-tie design methodology for three-dimensional reinforced concrete structures", *Journal of Structural Engineering*, vol. 132, no. 6, pp. 929–938, 2006, DOI: 10.1061/(ASCE)0733-9445(2006)132:6(929).

[10] V. Shobeiri and B. Ahmadi-Nedushan, "Bi-directional evolutionary structural optimization for strut-and-tie modelling of three-dimensional structural concrete", *Engineering Optimization*, vol. 49, no. 12, pp. 2055–2078, 2017, DOI: 10.1080/0305215X.2017.1292382.

[11] V. Shobeiri, "Determination of strut-and-tie models for structural concrete under dynamic loads", *Canadian Journal of Civil Engineering*, vol. 46, no. 12, pp. 1090–1102, 2019, DOI: 10.1139/cjce-2018-0780.

[12] M. Bruggi, "Generating strut-and-tie patterns for reinforced concrete structures using topology optimization", *Computers & Structures*, vol. 87, no. 23-24, pp. 1483-1495, 2009, DOI: 10.1016/j.compstruc.2009.06.003.

[13] Y. Xia, M. Langelaar, and M.A.N. Hendriks, "A critical evaluation of topology optimization results for strut-and-tie modeling of reinforced concrete", *Computer-Aided Civil and Infrastructure Engineering*, vol. 35, no. 8, pp. 850–869, 2020, DOI: 10.1111/mice.12537.

[14] W. Qiao and G. Chen, "Generation of strut-and-tie models in concrete structures by topology optimization based on moving morphable components", *Engineering Optimization*, vol. 53, no. 7, pp. 1251–1272, 2021, DOI: 10.1080/0305215X.2020.1781843.

[15] M. Victoria, O.M. Querin, and P. Martí, "Generation of strut-and-tie models by topology design using different material properties in tension and compression", *Structural and Multidisciplinary Optimization*, vol. 44, no. 2, pp. 247–258, 2011, DOI: 10.1007/s00158-011-0633-z.

[16] Z. Du, W. Zhang, Y. Zhang, et al., "Structural topology optimization involving bi-modulus materials with asymmetric properties in tension and compression", *Computational Mechanics*, vol. 63, no. 2, pp. 335–363, 2019, DOI: 10.1007/s00466-018-1597-2.

[17] O. Amir and O. Sigmund, "Reinforcement layout design for concrete structures based on continuum damage and truss topology optimization", *Structural and Multidisciplinary Optimization*, vol. 47, no. 2, pp. 157–174, 2013, DOI: 10.1007/s00158-012-0817-1.

[18] Y. Luo and Z. Kang, "Layout design of reinforced concrete structures using two-material topology optimization with Drucker–Prager yield constraints", *Structural and Multidisciplinary Optimization*, vol. 47, no. 1, pp. 95–110, 2013, DOI: 10.1007/s00158-012-0809-1.

[19] Z. Yang, K. Zhou, and S. Qiao, "Topology optimization of reinforced concrete structure using composite truss-like model", *Structural Engineering and Mechanics*, vol. 67, no. 1, pp. 79–85, 2018, DOI: 10.12989/sem.2018.67.1.079.

[20] H. Cui, L. Xie, M. Xiao, et al., "Conceptual design of reinforced concrete structures using truss-like topology optimization", *Archives of Civil Engineering*, vol. 68, no. 3, pp. 523–537, 2022, DOI: 10.24425/ace.2022.141900.

[21] K. Zhou and X. Li, "Topology optimization of truss-like continua with three families of members model under stress constraints", *Structural and Multidisciplinary Optimization*, vol. 43, no. 4, pp. 487–493, 2011, DOI: 10.1007/s00158-010-0584-9.

[22] H. Cui and K. Zhou, "Topology Optimization of Truss-Like Structure with Stress Constraints Under Multiple-Load Cases", *Acta Mechanica Solida Sinica*, vol. 33, no. 2, pp. 226–238, 2019, DOI: 10.1007/s10338-019-00125-3.

Received: 2022-08-24, Revised: 2022-11-03